arXiv:1704.06000v1 [stat.AP] 20 Apr 2017

Non-Coherent Direction-of-Arrival Estimation Using Partly Calibrated Arrays

Wassim Suleiman, Pouyan Parvazi, Marius Pesavento, and Abdelhak M. Zoubir

Abstract

In this paper, direction-of-arrival (DOA) estimation using non-coherent processing for partly calibrated arrays composed of multiple subarrays is considered. The subarrays are assumed to compute locally the sample covariance matrices of their measurements and communicate them to the processing center. A sufficient condition for the unique identifiability of the sources in the aforementioned non-coherent processing scheme is presented. We prove that, under mild conditions, with the non-coherent system of subarrays, it is possible to identify more sources than identifiable by each individual subarray. This property of non-coherent processing has not been investigated before. We derive the Maximum Likelihood estimator (MLE) for DOA estimation at the processing center using the sample covariance matrices received from the subarrays. Moreover, the Cramér-Rao Bound (CRB) for our measurement model is derived and is used to assess the presented DOA estimators. The behaviour of the CRB at high signal-to-noise ratio (SNR) is analyzed. In contrast to coherent processing, we prove that the CRB approaches zero at high SNR only if at least one subarray can identify the sources individually.

1. Introduction

DOA estimation using sensor arrays plays a fundamental role in many applications such as radar, sonar and seismic exploration [1]. Centralized subspace-based DOA estimation algorithms such as MUSIC [2], root-MUSIC [3], MODE [4], and WSF [5] exhibit the super-resolution property and are asymptotically efficient. These algorithms are applicable only when all sensor locations are known, i.e., the array is fully calibrated. For partly calibrated arrays with unknown displacements between the subarrays, subspace-based algorithms, such as ESPRIT [6], RARE [7] and algorithms proposed in [9] and [8], can be applied. These algorithms perform coherent processing, i.e, they require the covariance matrix of the whole array including the inter-subarray covariance matrices. Consequently, the subarrays are required to send their raw measurements to the processing center (PC) which then computes the overall array covariance matrix. Disadvantages encountered in coherent processing include the huge communication overhead at the subarrays and the high computational load at the PC.

Since, non-coherent processing techniques are carried out using only the subarray covariance matrices [10], the largest available covariance lag in non-coherent processing is the one corresponding to the subarray with the largest aperture, i.e., the subarray which possesses the largest inter-sensor distance. Whereas, in coherent processing, the largest available covariance lag corresponds to the whole array aperture which is larger than that of the individual subarrays. Thus, the DOA estimation performance of non-coherent processing is inferior to that of coherent-processing. Nevertheless, non-coherent processing is preferred in large wireless sensor networks since it offers a huge reduction in the communication overhead associated with communicating the raw subarray measurements to the PC as required in coherent processing. The computational load associated with non-coherent processing is also much smaller than that of the coherent processing, since only the small subarray covariance matrices are computed and not the large overall array covariance matrix. Thus, non-coherent processing is more convenient for decentralized processing [10]. Moreover, the computation of the inter-subarray covariance matrices in coherent processing requires synchronized subarrays, which is not always possible especially for widely separated subarrays [10]. Hence, in large arrays, it is necessary to resort to non-coherent processing. In such cases, the measurements of each subarray are processed coherently, namely the subarray covariance matrices are computed locally at the subarrays and communicated to the PC. Then, in the PC, non-coherent processing (using only local subarray covariance matrices) is carried out to achieve the DOA estimation task.

In [11, 12], the MUSIC algorithm is generalized to non-coherent processing where it is assumed that the subarrays locally estimate their noise subspaces and send them to the PC. In [13], another version of the MUSIC algorithm for non-coherent processing is analyzed. In this algorithm, the subarrays send the locally estimated DOAs and their estimated variances to the PC. A similar method which is robust against uncertainties in the statistical distribution of the noise is presented in [14]. In [10], it is proposed to perform DOA estimation using the MODE algorithm individually in each subarray. At the PC, the DOA estimates are optimally combined as in [13]. In [15], the root-MUSIC algorithm [3] is generalized for non-coherent processing where the subarrays locally compute the root-MUSIC polynomial coefficients and communicate them to the PC. Although the algorithms presented in [10–15] are designed for non-coherent processing, they all assume that each subarray can locally identify all the sources. Our primary goal in this paper is to overcome this restricting assumption.

In [16], direction finding using fewer receivers than the number of sources is introduced. Since only fewer receiver than the sources (and hence fewer than the sensors) are available, it is impossible to sample the output of all the sensors simultaneously. Thus, time varying processing is introduced where a different subset of the available sensors are sampled at each time period and their measurement covariance matrix is computed. The DOA estimation problem in this context can be considered as a non-coherent processing DOA estimation problem, since the covariance matrices between different sensor subsets are not available. However, the authors of [16] assume a fully calibrated array, whereas this assumption is not made in our paper. Moreover, the algorithms introduced in [16] perform an exhaustive search over the directions which is impractical when the number of sources is larger than two.

In this paper, DOA estimation using non-coherent processing for partly calibrated arrays is considered. We focus on the case where none of the subarrays is able to identify all the sources locally. We present a bound on the maximum number of identifiable sources. Using this bound, we show that for particular array geometries, it is possible to identify more sources than each subarray can identify individually. Thus, we achieve DOA estimation in more general scenarios than considered in [10–15].

Furthermore, two DOA estimation approaches are proposed: 1) the MLE and 2) a computationally simpler DOA estimation approach based on sparse signal representation (SSR). Moreover, the Cramér-Rao Bound (CRB) for our measurement model is presented and analyzed.

We remark that the non-coherent processing based DOA estimation approaches considered in this paper and in [10–15] differs from that presented in [17]. Where, in [17], DOA estimation is achieved from magnitude only measurements. Thus, the approach of [17] introduces ambiguities in DOA estimation which have been resolved by assuming sources at known locations. However, the approach of [17] assumes less information about the structure of the subarrays when compared to the approaches considered in this paper and in [10–15].

The remainder of the paper is organized as follows. In Section 2, the signal model is introduced. The case of uncorrelated sources is considered in Section 3. The model parameter identifiability is studied in Section 3.1. The MLE and the CRB are derived in Section 3.2 and in Section 3.3, respectively. DOA estimation based on the SSR approach is proposed in Section 3.4. In Section 4, the MLE and the CRB are extended to the case of correlated sources. In Section 5, simulation results are presented.

In this paper, lower-case bold symbols are used to denote vectors where upper-case bold symbols denote matrices. The transpose, complex conjugate, and the Hermitian operators are denoted as $(\cdot)^T$, $(\cdot)^*$, and $(\cdot)^H$, respectively. The symbols $\circ$ and $\otimes$ denote the Khatri-Rao and Kronecker products, respectively. The determinant and the trace of a matrix are denoted as $|\cdot|$ and $\mathrm{tr}\,(\cdot)$, respectively. The symbols $\boldsymbol{I}_i$, $\mathrm{diag}(\cdot)$, $\mathrm{blkdiag}(\cdot)$, $\mathrm{vec}(\cdot)$, $[\boldsymbol{A}]_{i,j}$, and $[\boldsymbol{a}]_i$ denote the identity matrix of size $i \times i$, diagonal matrices, block diagonal matrices, vectorization of a matrix, the (i,j)th entry of a matrix, and the ith entry of a vector, respectively. We write $\mathbf{1}_i$, $\mathbf{0}_i$, and $\boldsymbol{i}_k$ to denote the vector of all ones of size i, the vector of all zeros of size i, and vectorization of the identity matrix of size equal to the number of sensors at the kth subarray, respectively. The expectation of random variables, the floor operator, and the magnitude and angle of complex variables are denoted as $\mathbb{E}(\cdot)$, $\lfloor\cdot\rfloor$, $|\cdot|$, and $\angle\cdot$, respectively, where the imaginary unit is denoted as $\jmath$. The derivative of a function $f(x)$ with respect to a variable x is denoted as $\frac{df(x)}{dx}$.

2. Signal Model

We consider a planar partly calibrated array composed of K perfectly calibrated subarrays, i.e., for each subarray the following assumptions hold:

A1 the narrow-band assumption,

A2 the relative sensor locations are known,

A3 the sensors use a common sampling clock.

However, these assumptions do not hold between the subarrays. The kth subarray is comprised of M_k sensors, thus, the total number of sensors in the array is $M = \sum_{k=1}^{K} M_k$. We define $\boldsymbol{\zeta}_k \in \mathbb{R}^2$ as the vector containing the unknown displacement of the first sensor (reference) of the kth subarray and the reference sensor of the first subarray, thus, $\boldsymbol{\zeta}_1 = [0,0]^T$. The considered known relative position of the ith sensor of the kth subarray with respect to the first sensor of the kth subarray is denoted by $\boldsymbol{\zeta}'_{k,i}$, for $i = 1, \ldots, M_k$, and thus $\boldsymbol{\zeta}'_{k,1} = [0,0]^T$.

Signals of L narrow-band far-field sources impinge onto the array from directions $\boldsymbol{\theta} = [\theta_1, \ldots, \theta_L]^T$. The response of the kth subarray corresponding to a source at direction θ is given by

$$\boldsymbol{a}_k(\theta) = \boldsymbol{v}_k(\theta)\phi(\theta, \boldsymbol{\zeta}_k), \tag{1}$$

where $\phi(\theta, \boldsymbol{\zeta}_k) = \exp(\jmath \frac{2\pi}{\lambda_c} \boldsymbol{\zeta}_k^T \boldsymbol{\nu}(\theta))$ is an unknown phase shift, λ_c is the wavelength corresponding to the signal carrier frequency, and $\boldsymbol{\nu}(\theta) = [\sin(\theta), \cos(\theta)]^T$. The vector $\boldsymbol{v}_k(\theta)$ is defined as

$$\boldsymbol{v}_k(\theta) = [1, \exp(\jmath \frac{2\pi}{\lambda_c} \boldsymbol{\zeta}'^T_{k,2} \boldsymbol{\nu}(\theta)), \ldots, \exp(\jmath \frac{2\pi}{\lambda_c} \boldsymbol{\zeta}'^T_{k,M_k} \boldsymbol{\nu}(\theta))]^T. \tag{2}$$

In contrast to the phase shift $\phi(\theta, \boldsymbol{\zeta}_k)$, the vector $\boldsymbol{v}_k(\theta)$ is fully known as a function of θ.

The vector of the baseband signals received at the kth subarray is given by

$$\boldsymbol{x}_k(t - \tau_k) = \boldsymbol{A}_k(\boldsymbol{\theta}, \boldsymbol{\zeta}_k)\boldsymbol{s}(t - \tau_k) + \boldsymbol{n}_k(t - \tau_k) \tag{3}$$

where τ_k is the sampling offset at the kth subarray and $\boldsymbol{n}_k(t - \tau_k)$ is the vector containing the complex circular Gaussian sensor noise with zero-mean and variance σ^2. The vector $\boldsymbol{s}(t - \tau_k)$ contains the complex circular Gaussian source signals with zero-mean and covariance $\boldsymbol{P}$. We assume that the statistical properties of the sources observed by different subarrays are identical, i.e.,

$$\boldsymbol{P} = \mathbb{E}\big(\boldsymbol{s}(t - \tau_k)\boldsymbol{s}^H(t - \tau_k)\big), \tag{4}$$

for $k = 1, \ldots, K$. The steering matrix $\boldsymbol{A}_k(\boldsymbol{\theta}, \boldsymbol{\zeta}_k) = [\boldsymbol{a}_k(\theta_1, \boldsymbol{\zeta}_k), \ldots, \boldsymbol{a}_k(\theta_L, \boldsymbol{\zeta}_k)]^T$ is written as

$$\boldsymbol{A}_k(\boldsymbol{\theta}, \boldsymbol{\zeta}_k) = \boldsymbol{V}_k(\boldsymbol{\theta})\boldsymbol{\Phi}_k(\boldsymbol{\theta}, \boldsymbol{\zeta}_k), \tag{5}$$

where the matrix

$$\boldsymbol{V}_k(\boldsymbol{\theta}) = [\boldsymbol{v}_k(\theta_1), \ldots, \boldsymbol{v}_k(\theta_L)] \tag{6}$$

depends only on the DOAs, whereas the diagonal matrix

$$\boldsymbol{\Phi}_k(\boldsymbol{\theta}, \boldsymbol{\zeta}_k) = \operatorname{diag}\big(\phi_{k1}, \ldots, \phi_{kL}\big), \tag{7}$$

for $\phi_{kl} = \phi(\theta_l, \boldsymbol{\zeta}_k)$, depends on the DOAs and the unknown displacements in $\boldsymbol{\zeta}_k$. In the following, the dependency on $\boldsymbol{\theta}$ and $\boldsymbol{\zeta}_k$ is dropped for notation convenience.

The true measurement covariance matrix of the kth subarray is written as

$$\boldsymbol{R}_k = \mathbb{E}\big(\boldsymbol{x}_k(t-\tau_k)\boldsymbol{x}_k^H(t-\tau_k)\big) = \boldsymbol{V}_k\boldsymbol{\Phi}_k\boldsymbol{P}\boldsymbol{\Phi}_k^H\boldsymbol{V}_k^H + \sigma^2\boldsymbol{I}_{M_k}, \tag{8}$$

where the $M_k \times M_k$ identity matrix is denoted by $\boldsymbol{I}_{M_k}$ and $\boldsymbol{P}$ is defined in (4). For the later use, the source covariance matrix $\boldsymbol{P}$ is partitioned as

$$\boldsymbol{P} = \boldsymbol{\Lambda} + \boldsymbol{F}, \tag{9}$$

where the matrices $\boldsymbol{\Lambda}$ and $\boldsymbol{F}$ contain the diagonal and off-diagonal entries of the matrix $\boldsymbol{P}$, respectively. Denote the diagonal entries of the matrix $\boldsymbol{\Lambda}$ as λ_l, for $l = 1, \ldots, L$, then λ_l corresponds to the power of the lth source, $\lambda_l > 0$. We define

$$\boldsymbol{\lambda} = [\lambda_1, \ldots, \lambda_L]^T \tag{10}$$

to be the diagonal of the matrix $\boldsymbol{\Lambda}$. The (i,j)th entry of matrix $\boldsymbol{F}$, denoted as $[\boldsymbol{F}]_{i,j}$ corresponds to the correlation between the ith and jth sources. The ith and jth sources are coherent or fully correlated when $|[\boldsymbol{F}]_{i,j}| = \sqrt{\lambda_i \lambda_j}$.

The sample estimate of $\boldsymbol{R}_k$ is computed using N snapshots of the kth subarray output as

$$\hat{\boldsymbol{R}}_k = \frac{1}{N} \sum_{t=1}^{N} \boldsymbol{x}_k(t) \boldsymbol{x}_k^H(t), \tag{11}$$

where without loss of generality, we assume that the same number of samples N is available at all subarrays.

In this work, we assume that the subarrays send their locally estimated sample covariance matrices $\hat{\boldsymbol{R}}_k$, for $k = 1, \ldots, K$, to the PC[1], which carries out the DOA estimation algorithm. This processing type is referred to as *non-coherent processing* [10], since only the local subarray covariance matrices are available at the PC. Compared to *coherent processing* where the sample estimate of the cross-subarrays covariance matrices, i.e., $\mathbb{E}[\boldsymbol{x}_k(t)\boldsymbol{x}_i^H(t)]$, for $i \neq k$, $i, k =, 1 \ldots, K$, are available at the PC[2]. Which requires a synchronized subarray system, i.e., $\tau_k = 0$ for $k = 1, \ldots, K$. We remark that:

- In non-coherent processing, the resolution capability of the array is limited, compared to coherent processing, since the largest available covariance lag corresponds to the largest subarray. Whereas, in coherent processing, the largest available covariance lag corresponds to the array aperture.
- The non-coherent processing scheme is more suitable for decentralized processing than the coherent processing one, since each subarray can act as a decentralized processing node which computes the local covariance matrix of the subarray and sends it to the PC. Whereas, in coherent processing, the computation of the cross-subarray covariance matrices requires either sending the raw measurement to the PC or the use of the averaging consensus (AC) protocol, i.e., it involves a much larger communication overhead, see [18, 19].

3. DOA Estimation for Uncorrelated Sources

In this section, we consider the special case of perfectly uncorrelated sources for which the structure of the covariance matrix introduced in (8) can be simplified. We analyze the identifiability of our model and derive the CRB and the MLE. Moreover, DOA estimation using SSR is presented.

Under the assumption of uncorrelated sources, the source covariance matrix $\boldsymbol{P}$ in (4) is diagonal, i.e., the entries of the cross-correlation matrix $\boldsymbol{F}$ in (9) are zeros and $\boldsymbol{P} = \boldsymbol{\Lambda}$. Since the matrix $\boldsymbol{\Phi}_k$ is also diagonal with unit amplitude entries we can write

$$\boldsymbol{\Phi}_k \boldsymbol{P} \boldsymbol{\Phi}_k^H = \boldsymbol{P} = \boldsymbol{\Lambda}. \tag{12}$$

Substituting (12) in (8) yields

$$\boldsymbol{R}_k = \boldsymbol{V}_k \boldsymbol{\Lambda} \boldsymbol{V}_k^H + \sigma^2 \boldsymbol{I}_{M_k}. \tag{13}$$

In [20], the following matrix identity regarding the vectorization of the product of three matrices $\boldsymbol{M}_1, \boldsymbol{M}_2$, and $\boldsymbol{M}_3$ of appropriate sizes is proved:

$$\mathrm{vec}\big(\boldsymbol{M}_1 \boldsymbol{M}_2 \boldsymbol{M}_3\big) = (\boldsymbol{M}_3^T \otimes \boldsymbol{M}_1)\mathrm{vec}(\boldsymbol{M}_2). \tag{14}$$

Denote as $\boldsymbol{r}_k = \mathrm{vec}(\boldsymbol{R}_k)$ the vectorization of the kth subarray measurement covariance matrix. Then, substituting (13) and (14) in $\boldsymbol{r}_k$ yields

$$\boldsymbol{r}_k = \big(\boldsymbol{V}_k^* \otimes \boldsymbol{V}_k\big)\mathrm{vec}(\boldsymbol{\Lambda}) + \sigma^2 \boldsymbol{i}_k, \tag{15}$$

where $\boldsymbol{i}_k = \mathrm{vec}(\boldsymbol{I}_{M_k})$. Since $\boldsymbol{\Lambda}$ is a diagonal matrix, (15) is further reduced to

$$\boldsymbol{r}_k = \breve{\boldsymbol{V}}_k \boldsymbol{\lambda} + \sigma^2 \boldsymbol{i}_k, \tag{16}$$

[1]This requires sending M_k^2 real numbers to the PC, instead of $2NM_k$ in the case of sending raw measurements.

[2]Note that in the model (3), the computation of $\mathbb{E}[\boldsymbol{x}_k(t-\tau_k)\boldsymbol{x}_i^H(t-\tau_i)]$ when $k \neq i$ yields a covariance of zero if $|\tau_k - \tau_i|$ exceeds the coherence time of the signal waveforms such that $\mathbb{E}[\boldsymbol{s}(t-\tau_k)\boldsymbol{s}^H(t-\tau_i)] = \mathbf{0}_L \mathbf{0}_L^T$.

where the vector $\boldsymbol{\lambda}$ is defined in (10) and the $M_k^2 \times L$ matrix

$$\breve{\boldsymbol{V}}_k = \left(\boldsymbol{V}_k^* \circ \boldsymbol{V}_k\right) \tag{17}$$

contains the columns of the matrix $\left(\boldsymbol{V}_k^* \otimes \boldsymbol{V}_k\right)$ corresponding to the diagonal of $\boldsymbol{\Lambda}$. The matrix $\breve{\boldsymbol{V}}_k$ is referred as the co-subarray manifold[3]. We define the concatenation of all vectorized measurement covariance matrices as

$$\boldsymbol{r} = [\boldsymbol{r}_1^T, \ldots, \boldsymbol{r}_K^T]^T, \tag{18}$$

where $\boldsymbol{r}$ is of size $\breve{M} = \sum_{k=1}^{K} M_k^2$. By substituting (16) in (18), the vector $\boldsymbol{r}$ becomes

$$\boldsymbol{r} = \breve{\boldsymbol{V}}\boldsymbol{\lambda} + \sigma^2 \boldsymbol{i}, \tag{19}$$

where

$$\breve{\boldsymbol{V}} = [\breve{\boldsymbol{V}}_1^T, \ldots, \breve{\boldsymbol{V}}_K^T]^T \tag{20}$$

is the co-array manifold and

$$\boldsymbol{i} = [\boldsymbol{i}_1^T, \ldots, \boldsymbol{i}_K^T]^T. \tag{21}$$

We denote as $\hat{\boldsymbol{r}}$ and $\hat{\boldsymbol{r}}_k$, for $k = 1, \ldots, K$, the sample estimate of $\boldsymbol{r}$ and $\boldsymbol{r}_k$, respectively, which are obtained from the sample covariance matrix in (11).

3.1. Identifiability

In this subsection, we first revise the condition of parameter identifiability as introduced in [22], then we present a sufficient condition on the maximum number of identifiable (uncorrelated) sources.

Let $\boldsymbol{\theta}' = [\theta_1', \ldots, \theta_L']^T$ and $\boldsymbol{\theta}'' = [\theta_1'', \ldots, \theta_L'']^T$ denote two vectors each of them containing L pairwise-different DOAs. By pairwise-different DOA vector $\boldsymbol{\theta}'$ we mean that $\theta_i' \neq \theta_j'$ for $i \neq j$ and $i, j = 1, \ldots, L$. Then, we write $\boldsymbol{\theta}' \nsim \boldsymbol{\theta}''$ if there exist an index $i \leq L$ where for all $j \leq L$, $\theta_i' \neq \theta_j''$. In other words, at least one entry of $\boldsymbol{\theta}'$ is not equal to any entry of $\boldsymbol{\theta}''$. In the following, we present the definition of identifiability [22].

Definition 1 (Identifiability)**.** *In the noise free case, L sources with DOAs $\boldsymbol{\theta}$ and powers $\boldsymbol{\lambda}$ are uniquely identifiable if*

$$\breve{\boldsymbol{V}}(\boldsymbol{\theta})\boldsymbol{\lambda} \neq \breve{\boldsymbol{V}}(\boldsymbol{\theta}')\boldsymbol{\lambda}', \tag{22}$$

for any vector with positive entries $\boldsymbol{\lambda}'$ and for any pairwise-different DOA vector $\boldsymbol{\theta}'$, where $\boldsymbol{\theta} \nsim \boldsymbol{\theta}'$.

Note that in the noise free case, the product $\breve{\boldsymbol{V}}(\boldsymbol{\theta})\boldsymbol{\lambda}$ consist in the vectorized measurement covariances, i.e., $\boldsymbol{r} = \breve{\boldsymbol{V}}(\boldsymbol{\theta})\boldsymbol{\lambda}$. Let $F(\boldsymbol{x}(t)|\boldsymbol{\theta})$ denotes the distribution of the array measurements for a particular source directions $\boldsymbol{\theta}$. Since the subarray measurements follows a zero mean Gaussian distribution with (vectorized) covariances $\boldsymbol{r}$, Definition 1 implies that, the direction of the sources are uniquely identifiable if two parameter vectors $\boldsymbol{\theta}$ and $\boldsymbol{\theta}'$, where $\boldsymbol{\theta} \nsim \boldsymbol{\theta}'$, yield different measurement distributions, i.e., $F(\boldsymbol{x}(t)|\boldsymbol{\theta}) \neq F(\boldsymbol{x}(t)|\boldsymbol{\theta}')$ for $\boldsymbol{\theta} \nsim \boldsymbol{\theta}'$ [22].

Let ρ denotes the Kruskal rank [23,24] of the co-array manifold matrix $\breve{\boldsymbol{V}}$, i.e., ρ is the largest integer such that the columns of the matrix $\breve{\boldsymbol{V}}([\theta_1, \ldots, \theta_\rho]^T)$ are linearly independent for any vector $[\theta_1, \ldots, \theta_\rho]^T$ with pairwise different DOAs. Based on ρ, the following theorem provides a sufficient condition for the unique identifiability of L sources.

Theorem 1 (Sufficient condition for identifiability)**.** *The L DOAs $\boldsymbol{\theta}$ can be uniquely identified from covariances $\boldsymbol{r} = \breve{\boldsymbol{V}}\boldsymbol{\lambda}$ provided that*

$$L \leq \lfloor \frac{\rho}{2} \rfloor, \tag{23}$$

where ρ is the Kruskal rank of the co-array manifold $\breve{\boldsymbol{V}}$.

Proof. See Appendix A. □

[3]The expression co-array manifold have been used in [21] in the context of nonuniform linear antenna arrays to denote the Katri-Rao product of the conjugate array response with itself.

Denote by $\boldsymbol{b}_{k,i,j}$ the (i,j)th covariance lag of the kth subarray, i.e., $\boldsymbol{b}_{k,i,j} = \boldsymbol{\zeta}'_{k,j} - \boldsymbol{\zeta}'_{k,i}$ and let $\mathcal{B}_k$ denotes the set of all different covariance lags of the kth subarray, i.e.,

$$\mathcal{B}_k = \{\boldsymbol{b}_{k,i,j}, i,j = 1,\dots,M_k\}. \tag{24}$$

Further, let $\mathcal{B}$ denotes the set of different covariance lags of the whole array, i.e.,

$$\mathcal{B} = \bigcup_{k=1}^{K} \mathcal{B}_k. \tag{25}$$

Then the Kruskal rank ρ of the matrix $\breve{\boldsymbol{V}}$ is bounded by the number of covariance lags in the set $\mathcal{B}$. This observation yields the following result.

Corollary 1. *The number of sources which can be uniquely identified from covariances $\boldsymbol{r}$ is smaller than $\lfloor \mathrm{card}(\mathcal{B})/2 \rfloor$, where $\mathrm{card}(\mathcal{B})$ is the cardinality of the set $\mathcal{B}$.*

Corollary 1 implies that the number of uniquely identifiable sources using non-coherent processing can be increased by designing the subarrays with different covariance lags. Note that if all subarrays admit the same covariance lags, e.g., if the subarrays are identical, then the number of uniquely identifiable sources by the whole array is equal to the number identifiable by one individual subarray. The following example provides further insight.

Example

Consider an array composed of $K = 3$ identically oriented linear subarrays where the kth subarray includes $M_k = 2$ sensors. The relative positions between the successive sensors in the subarrays are assumed to be $d_1 = 1$, $d_2 = 2$ and $d_3 = 3$ half-wavelength, respectively, see Fig. 1. For coherent processing the maximum number of identifiable sources using this array is $M - K = 3$ (see [7]). Note that coherent processing scenario represents an upper bound on the number of uniquely identifiable sources using non-coherent processing, since more covariance lags are available for coherent processing, namely, the covariance lags corresponding to the relative position of two sensors belonging to different subarrays. Thus, $L \leq 3$ is a necessary condition for identifying the sources using non-coherent processing. In the following, based on Theorem 1, we show that $L \leq 3$ is a sufficient condition for identifying the sources in the considered array example.

The subarray steering vectors in (2) are reduced to $\boldsymbol{v}_k(\theta) = [1, e^{\jmath d_k \pi \sin\theta}]^T$, for $k = 1,\dots,3$, in this example. Thus, the matrix $\breve{\boldsymbol{V}}$ has the same rank as the matrix

$$\boldsymbol{W} = \begin{pmatrix} e^{-3\jmath\pi\sin\theta_1} & \dots & e^{-3\jmath\pi\sin\theta_L} \\ e^{-2\jmath\pi\sin\theta_1} & \dots & e^{-2\jmath\pi\sin\theta_L} \\ \vdots & \vdots & \vdots \\ e^{3\jmath\pi\sin\theta_1} & \dots & e^{3\jmath\pi\sin\theta_L} \end{pmatrix}, \tag{26}$$

where we only rearranged and deleted duplicated rows from $\breve{\boldsymbol{V}}$ to get $\boldsymbol{W}$. The matrix $\boldsymbol{W}$ is a Vandermonde matrix with 7 rows. Consequently, $\rho = 7$ and $\lfloor \frac{\rho}{2} \rfloor = 3$, i.e., up to $L = 3$ sources can be identified assuming non-coherent processing in this example. Thus, regarding identifiability non-coherent processing is equivalent to coherent processing in this scenario. Moreover, observe that where each subarray is able to identify one source locally (since each subarray consists of 2 sensors [25]), using non-coherent processing, the number of identifiable sources is increased up to $L = 3$ sources. This increase results from the fact that the three subarrays have different covariance lags.

3.2. Maximum Likelihood Estimator

In this section, the MLE for DOA estimation using non-coherent processing is derived considering uncorrelated sources.

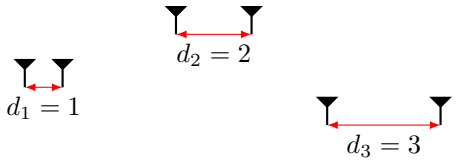

Figure 1: Array composed of $K = 3$ subarrays.

In the scenario considered in this work, the PC receives the sample covariance matrices from the subarrays. These matrices follow a Wishart distribution [26, p. 49] with probability density function (pdf)

$$\mathcal{P}(\hat{\boldsymbol{R}}_k) = \frac{|N\hat{\boldsymbol{R}}_k|^{N-M_k}}{\Gamma^c_{M_k}(N)|\boldsymbol{R}_k|^N} \exp\left(-N\text{tr}\left(\boldsymbol{R}_k^{-1}\hat{\boldsymbol{R}}_k\right)\right) \tag{27}$$

where $\Gamma^c_{M_k}(N) = \pi^{M_k(M_k-1)/2}\prod_{i=1}^{M_k}\prod_{j=1}^{N-i} j$ and $\boldsymbol{R}_k$ is given in (13). Ignoring the constant term in (27), the negative log-likelihood function is written as

$$\mathcal{L}(\boldsymbol{R}_1, \ldots, \boldsymbol{R}_K) = \sum_{k=1}^{K} N\left(\log|\boldsymbol{R}_k| + \text{tr}\left(\boldsymbol{R}_k^{-1}\hat{\boldsymbol{R}}_k\right)\right). \tag{28}$$

The function $\mathcal{L}(\boldsymbol{R}_1, \ldots, \boldsymbol{R}_K)$ is valid under the assumption of correlated sources as well as uncorrelated sources. Where only the structure of the measurement covariance matrices $\boldsymbol{R}_1, \ldots, \boldsymbol{R}_K$ depends on the source correlations. For uncorrelated sources the measurement covariance matrix of the kth subarray $\boldsymbol{R}_k$ reduces to (13), i.e., $\boldsymbol{R}_k$ depends on the DOAs $\boldsymbol{\theta}$, the source powers $\boldsymbol{\lambda}$, and the noise variance σ^2. Thus, the DOAs, the power of the sources, and the noise variance are estimated by solving the minimization problem

$$\begin{aligned} &\min_{\boldsymbol{\theta},\boldsymbol{\lambda},\sigma^2} \mathcal{L}(\boldsymbol{\theta}, \boldsymbol{\lambda}, \sigma^2) \\ &\text{s.t.} \quad \boldsymbol{\lambda} > \boldsymbol{0}_L, \\ &\qquad \sigma^2 > 0. \end{aligned} \tag{29}$$

The function $\mathcal{L}(\boldsymbol{\theta}, \boldsymbol{\lambda}, \sigma^2)$ in (29) is nonconvex [27]. Therefore, starting from a feasible point, a local solution (local minimum) for (29) can be computed, e.g., using the gradient descent method [27].

3.3. The Cramér-Rao Bound (CRB)

In [10], an expression for the CRB using non-coherent processing is derived under the assumption $M_k > L$, for $k = 1, \ldots, K$. Note that when $M_k < L$, the Fisher information matrix (FIM) corresponding to the kth subarray, denoted by FIM_k, is rank deficient. Therefore the expression of [10] is no longer valid. The FIM matrix for the non-coherent processing scenario

$$\text{FIM} = \sum_{k=1}^{K} \text{FIM}_k \tag{30}$$

is used to compute the CRB. Using (30) and following the steps of [16, 28], the CRB corresponding to the direction parameters $\boldsymbol{\theta}$ can be written as

$$\text{CRB}_{\boldsymbol{\theta}} = \left(\boldsymbol{\Delta}_1^H\left(\breve{\boldsymbol{R}} - \breve{\boldsymbol{R}}\boldsymbol{\Delta}_2\left(\boldsymbol{\Delta}_2^H\breve{\boldsymbol{R}}\boldsymbol{\Delta}_2\right)^{-1}\boldsymbol{\Delta}_2^H\breve{\boldsymbol{R}}\right)\boldsymbol{\Delta}_1\right)^{-1}. \tag{31}$$

where

$$\boldsymbol{\Delta}_1 = [\frac{d\boldsymbol{r}}{d\boldsymbol{\theta}^T}], \quad \boldsymbol{\Delta}_2 = [\frac{d\boldsymbol{r}}{d\boldsymbol{\lambda}^T}, \frac{d\boldsymbol{r}}{d\sigma^2}], \tag{32}$$

are the matrices which represent the derivatives of $\boldsymbol{r}$ with respect to $\boldsymbol{\theta}$, $\boldsymbol{\lambda}$, and σ^2, respectively,

$$\breve{\boldsymbol{R}} = \text{blkdiag}\left(\breve{\boldsymbol{R}}_1, \ldots, \breve{\boldsymbol{R}}_K\right), \tag{33}$$

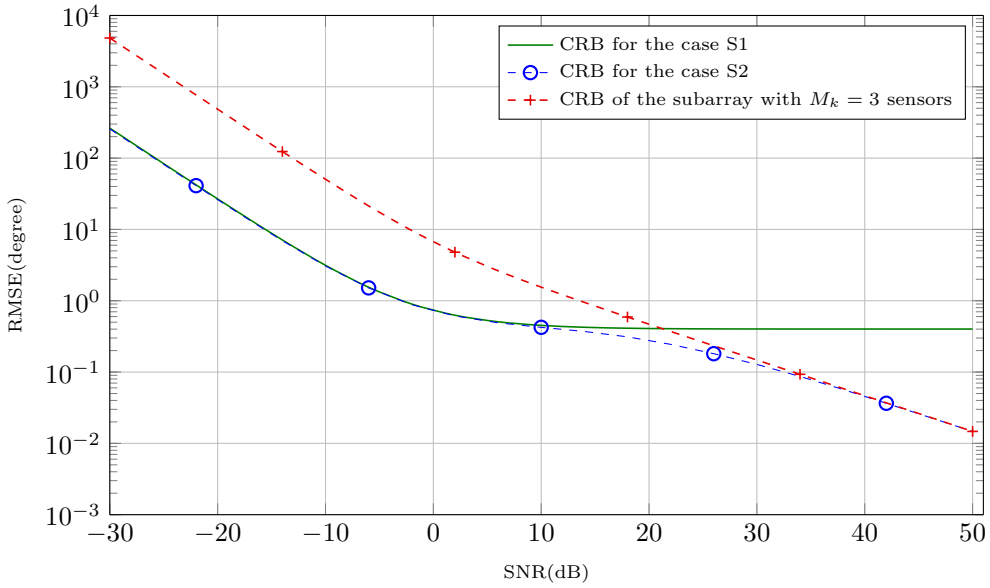

Figure 2: The CRB for the cases where 1) none of the subarrays are able to identify the sources individually 2) one subarray can identify the sources. Also the CRB for the subarray with 3 sensors in case 2) is shown.

and $\breve{\boldsymbol{R}}_k = N(\boldsymbol{R}_k^{-T} \otimes \boldsymbol{R}_k^{-1})$. In the sequel, we demonstrate the behaviour of the CRB at high SNR by simulation and we analyze this behaviour.

Consider the following two scenarios:

S1 $M_1 = \cdots = M_K \leq L$, i.e., the FIM for each individual subarray is not invertible, whereas the overall FIM, defined in (30), is invertible.

S2 $M_1 > L$ and $M_k \leq L$, for $k = 2, \ldots, K$, i.e., the FIM of the first subarray FIM_1 is invertible whereas the FIM of the remaining subarrays, i.e., FIM_k, for $k = 2, \ldots, K$ are not invertible.

In Fig. 2, we display the CRB for $K = 12$ subarrays and $L = 2$ uncorrelated equal-power sources for two array configurations which represent the aforementioned scenarios S1 and S2[4]:

1. $M_1 = \cdots = M_K = 2 = L$, which represents S1.
2. $M_1 = 3 > L$ and $M_2 = \cdots = M_{K-1} = 2 = L$, which represents S2.

Moreover, in Fig. 2, we display the CRB of the first subarray with $M_1 = 3$ sensors. It can be observed from Fig. 2 that in the scenario S1, the CRB does not approach zero as the SNR approaches infinity rather it remains unchanged at high SNR (in Fig. 2, the CRB remains almost unchanged for SNR above 15 dB). In the scenario S2, the CRB is almost identical to that of the scenario S1 when the SNR is less than 15 dB. However, it continues to decrease for SNR larger than 15 dB and the performance at high SNR in this case is determined by the performance of the first subarray. Thus, at high SNR, DOA estimation can be performed using only those subarrays which are able to identify and estimate the DOAs individually, if such subarrays exist. In [14], the authors suggested to include only subarrays which can individually identify all the sources in the DOA estimation algorithm. This approach is justified at high SNR, however, at low SNR using all the subarray yields the better estimation performance, as demonstrated by the CRB in Fig. 2.

In the following, we analyze the aforementioned behaviour of the CRB at high SNR in the two scenarios S1 and S2. Thus, we consider L uncorrelated equally-powered sources in the high SNR region, i.e., $\lambda_1 = \cdots = \lambda_L = \lambda$, where $\lambda_1, \ldots, \lambda_L$ are the power of the sources whose directions are denoted by $\theta_1, \ldots, \theta_L$, respectively, and $\lambda \gg \sigma^2$, refer to (10). Let $\boldsymbol{r}|_{\lambda \gg \sigma^2} = \lambda \left(\breve{\boldsymbol{V}} \mathbf{1}_L + \frac{\sigma^2}{\lambda} \boldsymbol{i} \right)|_{\lambda \gg \sigma^2} \approx \lambda \breve{\boldsymbol{V}} \mathbf{1}_L$ denotes the high

[4]For the details on the array geometry parameters please refer the array setup described in Section 5.

SNR approximation of the vectorized covariance matrices. Consequently, the derivative matrices $\boldsymbol{\Delta}_1$ and $\boldsymbol{\Delta}_2$ in (32) reduce to $\boldsymbol{\Delta}_1|_{\lambda\gg\sigma^2} = \lambda[\frac{d(\breve{\boldsymbol{V}}\mathbf{1}_L)}{d\boldsymbol{\theta}^T}]$ and $\boldsymbol{\Delta}_2|_{\lambda\gg\sigma^2} = [\breve{\boldsymbol{V}}\mathbf{1}_L, \boldsymbol{i}]$. Similarly, we denote $\breve{\boldsymbol{R}}$ at high SNR by $\breve{\boldsymbol{R}}|_{\lambda\gg\sigma^2} \approx \lambda^{-2}N\overline{\boldsymbol{V}}$, where $\overline{\boldsymbol{V}} = \text{blkdiag}\left(\overline{\boldsymbol{V}}_1, \ldots, \overline{\boldsymbol{V}}_K\right)$ and $\overline{\boldsymbol{V}}_k = (\boldsymbol{V}_k\boldsymbol{V}_k^H)^{-T} \otimes (\boldsymbol{V}_k\boldsymbol{V}_k^H)_k^{-1}$. Substituting $\boldsymbol{\Delta}_1|_{\lambda\gg\sigma^2}$, $\boldsymbol{\Delta}_2|_{\lambda\gg\sigma^2}$, and $\breve{\boldsymbol{R}}|_{\lambda\gg\sigma^2}$ in (31) the CRB in the high SNR region reduces to

$$\text{CRB}_{\boldsymbol{\theta}}^{-1}|_{\lambda\gg\sigma^2} \approx N[\frac{d(\breve{\boldsymbol{V}}\mathbf{1}_L)}{d\boldsymbol{\theta}^T}]^H\, \overline{\boldsymbol{V}}\, [\frac{d(\breve{\boldsymbol{V}}\mathbf{1}_L)}{d\boldsymbol{\theta}^T}]. \tag{34}$$

Interestingly, we observe from (34) that at high SNR, the expression for $\text{CRB}_{\boldsymbol{\theta}}^{-1}|_{\lambda\gg\sigma^2}$ depend neither on λ nor on σ^2 but only on the DOAs $\theta_1, \ldots, \theta_L$. Next, let us consider how the expression for $\text{CRB}_{\boldsymbol{\theta}}^{-1}|_{\lambda\gg\sigma^2}$ changes in the two scenarios S1 and S2. Let $\overline{\rho}_k$ denote the rank of the matrix $\overline{\boldsymbol{V}}_k^{-1}$. Since the rank of the Kronecker product is the product of the ranks of its operand matrices [29], the rank $\overline{\rho}_k$, for $k = 1, \ldots, K$, takes the value $\overline{\rho}_k = M_k^2$ in both scenarios S1 and S2[5]. Thus, the following behaviour of the block diagonal matrix $\overline{\boldsymbol{V}}^{-1}$ is observable:

- In the scenario S1, $\overline{\boldsymbol{V}}^{-1}$ is full rank.
- In the scenario S2, $\overline{\boldsymbol{V}}^{-1}$ is rank deficient. More precisely, the first block of $\overline{\boldsymbol{V}}^{-1}$, which corresponds to the first subarray is rank deficient.

Consequently, in the scenario S1, the matrix $\overline{\boldsymbol{V}}$ has finite entries (and eigenvalues) leading to a finite non-zero CRB. Whereas, in the scenario S2, the matrix $\overline{\boldsymbol{V}}$ has infinitely large eigenvalues which asymptotically drive the CRB to zero). Moreover, in the scenario S2, $\text{CRB}_{\boldsymbol{\theta}}^{-1}|_{\lambda\gg\sigma^2}$ in (34) can be approximated by $N[\frac{d(\breve{\boldsymbol{V}}_1\mathbf{1}_L)}{d\boldsymbol{\theta}^T}]^H\, \overline{\boldsymbol{V}}_1\, [\frac{d(\breve{\boldsymbol{V}}_1\mathbf{1}_L)}{d\boldsymbol{\theta}^T}]$ since the entries of $\overline{\boldsymbol{V}}_2, \ldots, \overline{\boldsymbol{V}}_K$ are negligible compared to the entries of $\overline{\boldsymbol{V}}_1$. Which means that in the scenario S2, at high SNR, the CRB of the whole array can be approximated by the CRB of the first subarray. We remark that a behaviour of the CRB similar to that of scenario S1 at high SNR has been observed in [16, 28] for DOA estimation using fewer receivers and "it is shown to be typical in scenarios where a signal subspace is nonexistent". However, in [16, 28] the scenario S2 has not been considered. Moreover, in [30, Fig. 1], a similar behaviour to the scenario S1 is observed in DOA estimation using fully augmentable sparse linear arrays when the number of sources is larger than the number of the sensors in the array but smaller than the available covariance lags.

Regarding the number of samples N, we point out that the CRB approaches zero in both scenarios S1 and S2 when N approaches infinity, as it can be observed from (34).

3.4. DOA Estimation Using Sparse Signal Representation

Sparse signal representation (SSR) [31–35] has recently attracted much attention in DOA estimation applications, see [36–40]. One important advantage of SSR is that it performs well in the low sample size regime. Furthermore, using the norm ℓ_1 relaxation the SSR can be cast as a convex optimization problem. So far, the focus of DOA estimation using SSR has been in the context of coherent processing [36–40], however, to the best of our knowledge the SSR approach has not yet been applied for non-coherent processing based DOA estimation. In this section, we formulate the DOA estimation problem in the case of uncorrelated sources as a SSR problem, which can be solved using convex optimization algorithms, see [27, 41].

For coherent processing using fully calibrated array, covariance based SSR approaches for deterministic and stochastic source models are introduced in [42] and [43], respectively. Since a stochastic source model is assumed in this paper, we extend the approach of [43], referred to as SParse Iterative Covariance-based approach (SPICE), to non-coherent processing using partly calibrated arrays[6].

Let $\tilde{\boldsymbol{\theta}}$ be the vector of length G obtained by sampling the field-of-view in $G \gg L$ angular directions

$$\tilde{\boldsymbol{\theta}} = [\tilde{\theta}_1, \ldots, \tilde{\theta}_G]^T. \tag{35}$$

[5] Using the well-known inversion identity $(\boldsymbol{A} \otimes \boldsymbol{B})^{-1} = \boldsymbol{A}^{-1} \otimes \boldsymbol{B}^{-1}$ [29].

[6] The extension of [42] to non-coherent processing using partly calibrated arrays is similar to that of [43].

Then, the SPICE optimization problem [43, Equation (20)] for the considered non-coherent processing scenario is written as

$$\min_{\tilde{\boldsymbol{\lambda}},\sigma^2} \sum_{k=1}^{K} \mathrm{tr}\left(\tilde{\boldsymbol{R}}_k^{-1}\hat{\boldsymbol{R}}_k\right) \tag{36a}$$

$$\text{s.t.} \quad \tilde{\boldsymbol{\lambda}} \geq \mathbf{0}_G,\ \sigma^2 \geq 0, \tag{36b}$$

$$\sum_{g=1}^{G} w_g \tilde{\lambda}_g + \overline{w}\sigma^2 = 1 \tag{36c}$$

where $\tilde{\boldsymbol{R}}_k = \tilde{\boldsymbol{V}}_k \tilde{\boldsymbol{\Lambda}} \tilde{\boldsymbol{V}}^H + \sigma^2 \boldsymbol{I}_{M_k}$ and the $\breve{M}_k \times G$ overcomplete dictionary $\tilde{\boldsymbol{V}}_k$ is defined as

$$\tilde{\boldsymbol{V}}_k = [\boldsymbol{v}_k(\tilde{\boldsymbol{\theta}}_1), \ldots, \boldsymbol{v}_k(\tilde{\boldsymbol{\theta}}_G)]. \tag{37}$$

The diagonal matrix $\tilde{\boldsymbol{\Lambda}}$ is a sparse matrix whose diagonal elements, denoted as $\tilde{\boldsymbol{\lambda}}$, correspond to the powers of the sources at directions $\tilde{\boldsymbol{\theta}}$. The weights in (36c) are defined as

$$w_g = \frac{1}{M}\sum_{k=1}^{K} \boldsymbol{v}_k^H(\tilde{\boldsymbol{\theta}}_g)\hat{\boldsymbol{R}}_k^{-1}\boldsymbol{v}_k(\tilde{\boldsymbol{\theta}}_g), \tag{38}$$

and

$$\overline{w} = \frac{1}{M}\sum_{k=1}^{K} \mathrm{tr}\left(\hat{\boldsymbol{R}}_k^{-1}\right). \tag{39}$$

In [43], it has been pointed out that the constraint (36c) is a weighted ℓ_1 norm and thus is expected to induce sparsity. Note that in contrast to other ℓ_1 norm based DOA estimation approaches, the SPICE approach does not require the configuration of a sparsity regularization parameter. Problem (36) is positive semi-definite [43] thus can be solved using, e.g., cvx [41][7].

Note that using SSR, the DOA estimation problem is reduced to the identification of the non-zero elements in the estimated sparse vector $\hat{\tilde{\boldsymbol{\lambda}}}$. These non-zero elements are referred to as the support set of $\hat{\tilde{\boldsymbol{\lambda}}}$. The DOA estimates are the grid points, i.e., the elements of $\tilde{\boldsymbol{\theta}}$, which correspond to the L largest peaks of $\hat{\tilde{\boldsymbol{\lambda}}}$.

4. Extension to Correlated Sources

In the previous section, we assumed that the sources impinging onto the system of subarrays are uncorrelated. In this case, the source covariance matrix satisfies (12) and the measurement covariance matrix reduces to (13). However, by dropping the assumption of uncorrelated sources, (12) is no longer valid since the matrix $\boldsymbol{F}$, defined in (9), is non-zero. In this section, we extend the MLE, the SSR approach, and the CRB which have been introduced in the previous section for the case of uncorrelated sources to the case of correlated sources.

4.1. The MLE and SSR approaches for Correlated Sources

The derivation of the MLE in the correlated sources case is similar to the case of uncorrelated sources, which is introduced in Section 3.2. However, in this case, the off-diagonal entries of the source covariance matrix $\boldsymbol{P}$ are non-zero. Consequently, the property (12) does not hold. Thus, in contrast to (13), the measurement covariance matrix $\boldsymbol{R}_k$ for correlated sources, defined in (8), depends on the unknown displacements between the subarrays, represented by the matrix $\boldsymbol{\Phi}_k$ for $k = 1, \ldots, K$. The negative log-likelihood in the presence of correlated sources, denoted as $\mathcal{L}(\boldsymbol{\theta}, \boldsymbol{P}, \sigma^2, \boldsymbol{\Phi}_2, \ldots, \boldsymbol{\Phi}_K)$, is defined in (28). However, for $\mathcal{L}(\boldsymbol{\theta}, \boldsymbol{P}, \sigma^2, \boldsymbol{\Phi}_2, \ldots, \boldsymbol{\Phi}_K)$

[7] Problem (36) can be cast as second order cone program (SOCP) and it can be extended to the case where the sensor noise variance are not identical at all sensors, see [43].

the covariance matrix as defined in (8) is used since (13) is only valid for uncorrelated source. The DOAs can be estimated from the minimization problem

$$\begin{aligned} &\min_{\boldsymbol{\theta},\boldsymbol{P},\sigma^2,\boldsymbol{\Phi}_1,\ldots,\boldsymbol{\Phi}_K} \mathcal{L}(\boldsymbol{\theta},\boldsymbol{P},\sigma^2,\boldsymbol{\Phi}_1,\ldots,\boldsymbol{\Phi}_K) \\ &\text{s.t.} \quad \boldsymbol{P} \succeq 0, \\ &\qquad \sigma^2 > 0, \end{aligned} \tag{40}$$

where $\boldsymbol{P} \succeq 0$ denotes that the matrix $\boldsymbol{P}$ is positive semidefinite. Similar to the case of uncorrelated sources, the optimization problem (40) is nonconvex. Therefore, starting from a feasible point, a local solution (local minimum) for (40) can be computed, e.g., using the gradient descent method [27].

We remark that the SSR approach introduced in Section 3.4 for uncorrelated sources is robust to the assumption of uncorrelated sources. This robustness results from the fact that the SPICE method, which we base our SSR approach on, is robust to the assumption of uncorrelated sources [43, Section II]. Consequently, the SSR approach as introduced in Section 3.4 for uncorrelated sources is applicable in the case of correlated sources.

4.2. The CRB for Correlated Sources

The derivation of the CRB for the case of correlated sources is similar to the case of uncorrelated sources. The CRB for the case of correlated sources is written as in (31) with $\boldsymbol{\Delta}_2$ defined as

$$\boldsymbol{\Delta}_2 = [\frac{d\boldsymbol{r}}{d\boldsymbol{p}^T}, \frac{d\boldsymbol{r}}{d\sigma^2}, \frac{d\boldsymbol{r}}{d\boldsymbol{\zeta}_2^T}, \ldots, \frac{d\boldsymbol{r}}{d\boldsymbol{\zeta}_K^T}], \tag{41}$$

where $\boldsymbol{p}$ is a real vector of length L^2 which represents the unknown parameters of the source covariance matrix. More precisely $\boldsymbol{p}$ contains the diagonal of $\boldsymbol{P}$ and the real and imaginary parts of the upper diagonal of the matrix $\boldsymbol{P}$. In the following, we demonstrate the behaviour of the CRB at high SNR by simulation and we carry out an asymptotic (for high SNR) analysis of this behaviour.

Example

In Fig. 3, we display the CRB for $K = 12$ subarrays each consists of two sensors and $L = 2$ equally-powered correlated sources,[8] i.e., the matrix FIM_k, for $k = 1, \ldots, K$, are not invertible. Thus, the source covariance matrix is

$$\boldsymbol{P} = \lambda\, \boldsymbol{\Upsilon} \tag{42}$$

where $\boldsymbol{\Upsilon} = \begin{bmatrix} 1 & \epsilon \\ \epsilon^* & 1 \end{bmatrix}$, the correlation factor ϵ satisfies $0 \leq |\epsilon| \leq 1$, and λ is the power of each of the two sources. In Fig. 3, the CRB is displayed for correlation factor ϵ of $0, 0.3, 0.6$, and 1, where the latter correlation value indicates coherent sources. Observe in Fig. 3 that the CRB of the estimated DOAs for correlated sources behaves similar to the uncorrelated sources case of Fig. 2. However, the CRB decreases with the increase of ϵ. Interestingly, for coherent sources, i.e., for $\epsilon = 1$, the CRB approaches zero at high SNR, which is in exact contrast to the case of uncorrelated or partly correlated sources where the CRB does not vanish with SNR.

In the sequel, the aforementioned behaviour of the CRB is analyzed asymptotically for high SNR values. Following the steps of Section 3.3 for the case of uncorrelated sources, in the correlated source case the CRB at high SNR is written as

$$\mathrm{CRB}_{\boldsymbol{\theta}}^{-1}|_{\lambda \gg \sigma^2} \approx N[\frac{d\boldsymbol{u}}{d\boldsymbol{\theta}^T}]^H\, \overline{\overline{\boldsymbol{V}}}\, [\frac{d\boldsymbol{u}}{d\boldsymbol{\theta}^T}], \tag{43}$$

where $\boldsymbol{u} = [\boldsymbol{u}_1^T, \ldots, \boldsymbol{u}_K^T]^T$, $\boldsymbol{u}_k = \mathrm{vec}(\boldsymbol{V}_k \boldsymbol{\Phi}_k \boldsymbol{\Upsilon} \boldsymbol{\Phi}_k^H \boldsymbol{V}_k^H)$, $\overline{\overline{\boldsymbol{V}}} = \mathrm{blkdiag}\left(\overline{\overline{\boldsymbol{V}}}_1, \ldots, \overline{\overline{\boldsymbol{V}}}_K\right)$, and $\overline{\overline{\boldsymbol{V}}}_k = (\boldsymbol{V}_k \boldsymbol{\Phi}_k \boldsymbol{\Upsilon} \boldsymbol{\Phi}_k^H \boldsymbol{V}_k^H)^{-T} \otimes (\boldsymbol{V}_k \boldsymbol{\Phi}_k \boldsymbol{\Upsilon} \boldsymbol{\Phi}_k^H \boldsymbol{V}_k^H)^{-1}$. Note that $\mathrm{CRB}_{\boldsymbol{\theta}}^{-1}|_{\lambda \gg \sigma^2}$ depends neither on λ nor on σ^2. Thus, based on the rank of the matrix $\overline{\overline{\boldsymbol{V}}}_k^{-1}$, denoted as $\overline{\rho}_k$, the following two cases are distinguished:

[8] The same configuration as in the case S1 in Section 3.1, expect for the source correlation, is used. For the details on the array geometry parameters please refer the array setup described in Section 5.

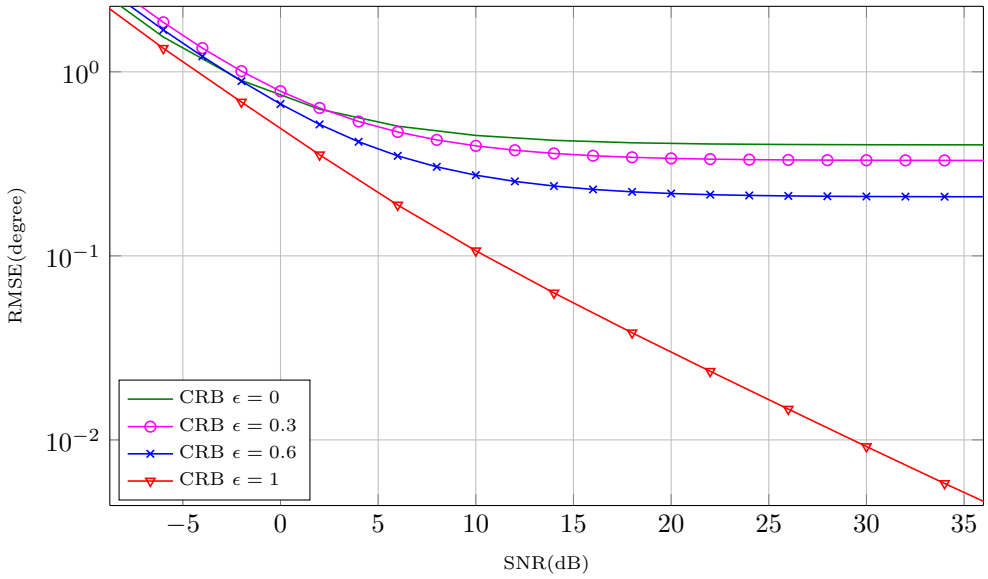

Figure 3: The CRB in the case of correlated sources for different source correlation ϵ.

1) The case when $|\epsilon| < 1$ in which $\overline{\rho}_k = M_k^2$, for $k = 1, \ldots, K$, consequently, the matrix $\overline{\overline{\boldsymbol{V}}}^{-1}$ is full rank, and the CRB does not vanish at high SNR.

2) The case when $|\epsilon| = 1$ in which $\overline{\rho}_1 = \cdots \overline{\rho}_K = 1$, consequently, the matrix $\overline{\overline{\boldsymbol{V}}}^{-1}$ is rank deficient and asymptotically drives the CRB to zero at high SNR.

5. Simulation Results

In this section, we analyze the performance of our proposed MLE and SSR estimation methods using simulations for both cases uncorrelated and correlated sources. The cvx [41] framework is used to solve the SPICE optimization problem in (36), where the the field-of-view is sampled every 0.1°.

The MLE is initialized with the solution of the SPICE method and the MATLAB command *fmincon* is used to compute the MLE as presented in (29) and (40) for uncorrelated and correlated sources, respectively.

In our simulations, an array composed of $K = 12$ subarrays each is comprised of 2 sensors is considered. The location of the first sensors in the 12 subarrays measured in half-wavelength are $(0, 0)$, $(17.3, 6)$, $(-2.4, 6.2)$, $(10.5, -2)$, $(12.7, 2.1)$, $(4.6, -2.4)$, $(4.6, 4.5)$, $(4.5, 5.3)$, $(2.3, 9)$, $(10.2, 8.1)$, $(10.2, 4)$, and $(13.4, 6)$. These locations are considered to be unknown during the DOA estimation process. The locations of the second sensors in each subarray with respect to the first sensor in the corresponding subarray measured in half-wavelength are $(6.5, 0)$, $(4.4, 0)$, $(3.5, 0)$, $(2.6, 0)$, $(2.6, 0)$, $(2.5, 0)$, $(1.9, 0)$, $(1.5, 0)$, $(1.4, 0)$, $(1.3, 0)$, $(1, 0)$, and $(0.5, 0)$. These locations are considered to be known. Signals of two far-field equal-powered uncorrelated sources are impinging onto the subarrays from directions -11.4° -1.1°. In our simulations, the root mean square error (RMSE) for the estimated DOAs is computed over 100 realizations as

$$\Big(\frac{1}{100}\sum_{i=1}^{100}\frac{1}{L}\sum_{l=1}^{L}(\hat{\theta}_l(i) - \theta_l)^2\Big)^{1/2}, \tag{44}$$

where $\hat{\theta}_l(i)$ is the estimate of the lth DOA at realization i. The RMSE in (44) is computed for the SPICE and the MLE approaches. We also display the CRB computed as

$$\Big(\frac{1}{L}\sum_{i=1}^{L}[\mathrm{CRB}_{\boldsymbol{\theta}}]_{l,l}\Big)^{1/2}, \tag{45}$$

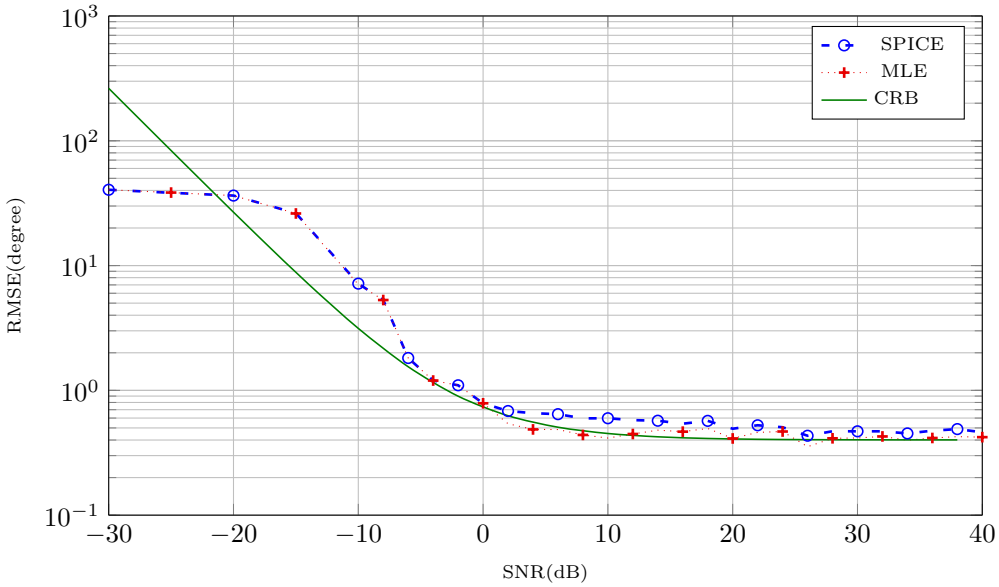

(a)

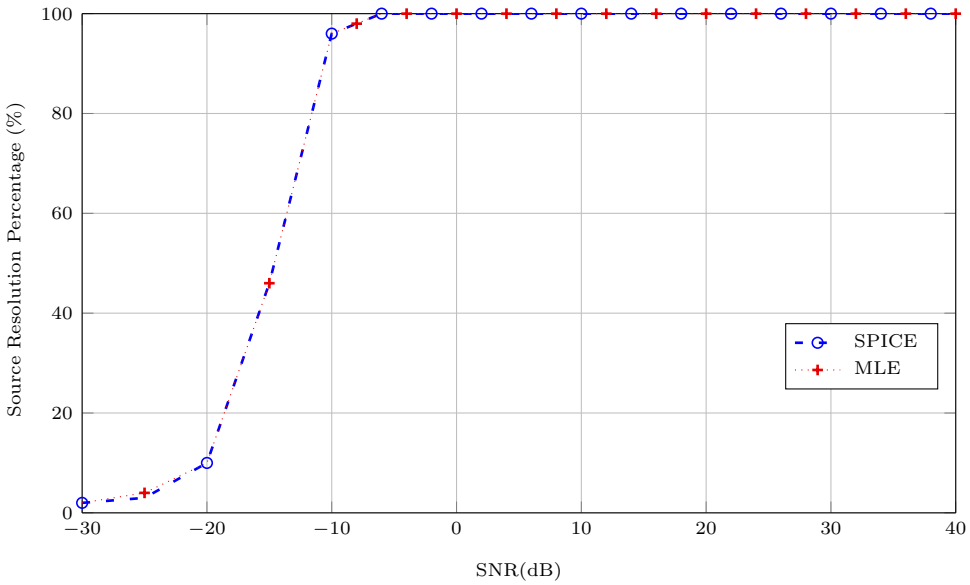

(b)

Figure 4: DOA estimation performance, assuming uncorrelated sources, plotted against SNR for a fixed number of samples $N = 50$: (a) the RMSE of the proposed DOA estimation methods averaged over 100 realizations, (b) the resolution percentage of the proposed DOA estimation methods averaged over 100 realizations.

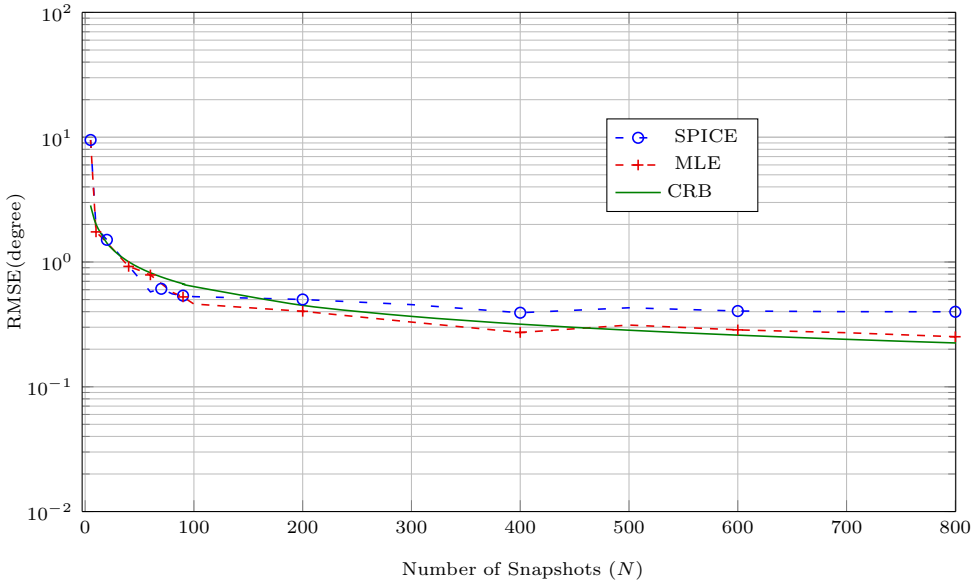

(a)

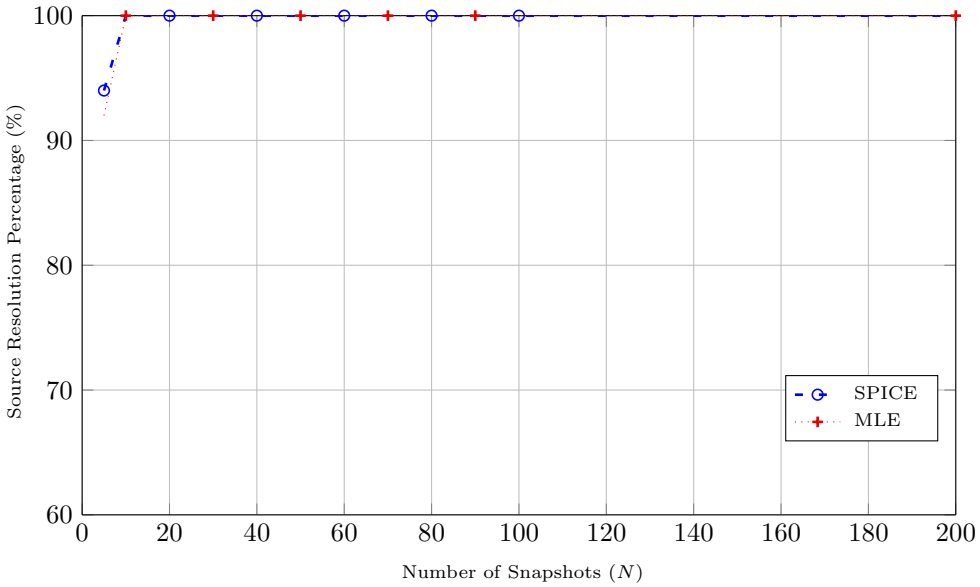

(b)

Figure 5: DOA estimation performance, assuming uncorrelated sources, plotted against the number of snapshots N for a fixed SNR= -2 dB: (a) the RMSE of the proposed DOA estimation methods averaged over 100 realizations, (b) the resolution percentage of the proposed DOA estimation methods averaged over 100 realizations.

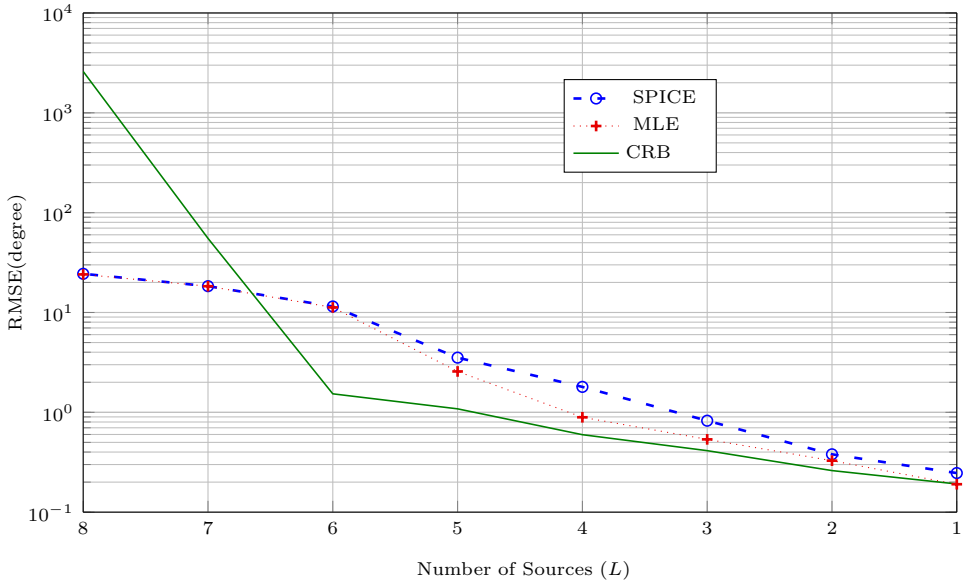

(a)

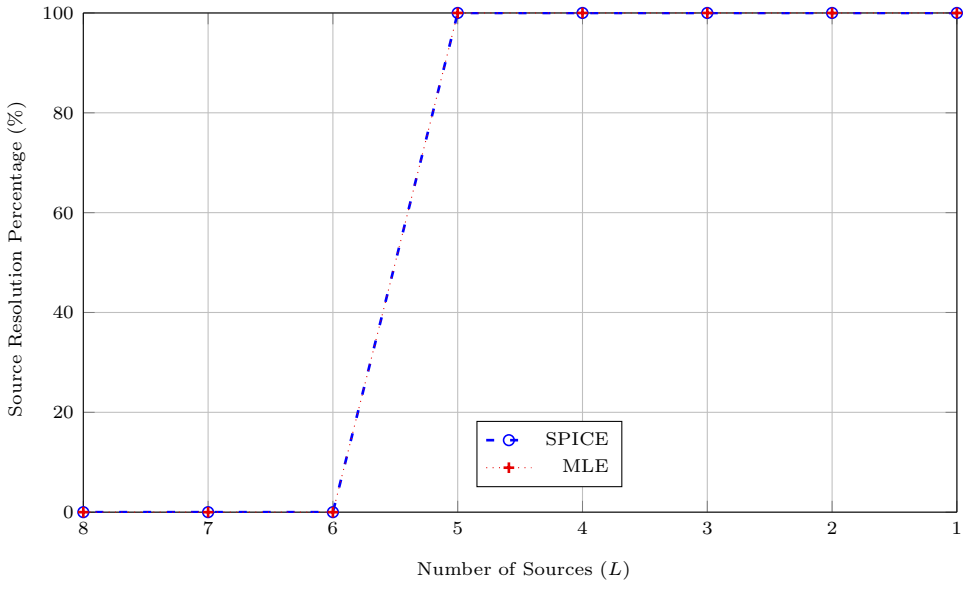

(b)

Figure 6: DOA estimation performance, assuming uncorrelated sources, plotted against the number of sources L for a fixed number of samples $N = 50$ and a fixed SNR$= -2$ dB: (a) the RMSE of the proposed DOA estimation methods averaged over 100 realizations, (b) the resolution percentage of the proposed DOA estimation methods averaged over 100 realizations.

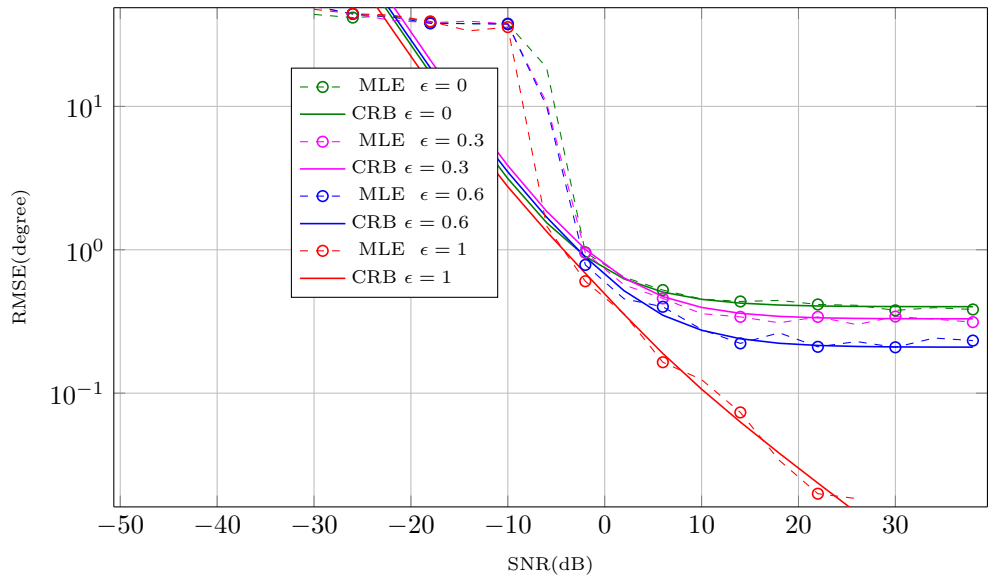

(a)

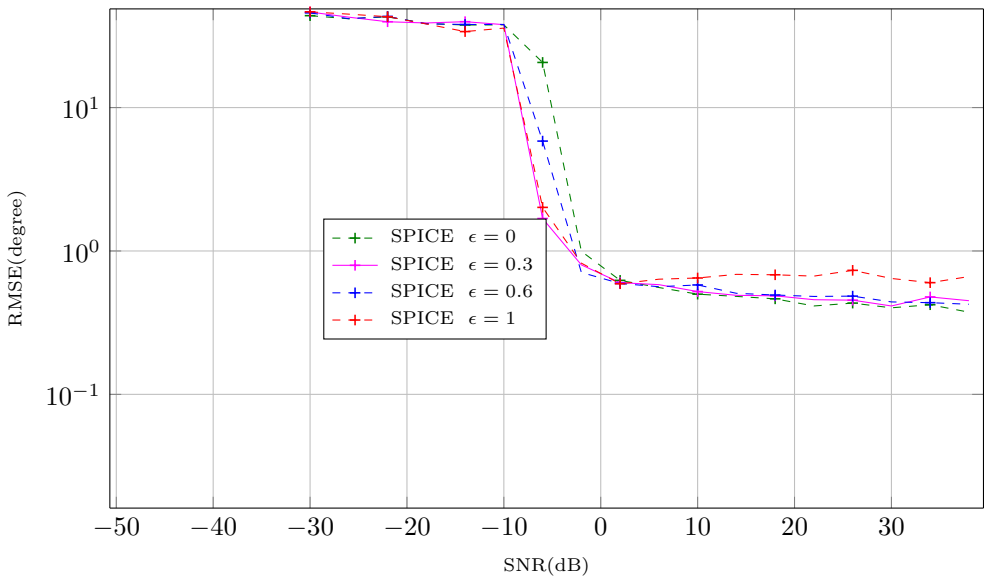

(b)

Figure 7: RMSE for correlated sources as a function of SNR for a fixed number of samples $N = 50$ for different values of the correlation factor ϵ: (a) the averaged RMSE for the MLE approach, (b) the averaged RMSE for the SPICE approach.

where $[\mathrm{CRB}_{\boldsymbol{\theta}}]_{l,l}$ is the lth diagonal entry of the matrix $\mathrm{CRB}_{\boldsymbol{\theta}}$.

In Fig. 4a, the averaged performance of the SPICE and the MLE for a fixed number of samples $N = 50$ is plotted against SNR. It can be observed in Fig. 4a that the MLE and the SPICE method achieves the CRB at high SNR. In Fig. 4b, the source resolution percentage of the considered DOA estimation methods is plotted against the SNR, where two sources are considered to be resolved if the error in the estimated DOAs is less than half of the angular separation between the two sources [9]. Observe that for SNR ≥ -8 dB, the MLE and SPICE method can always identify the sources and for SNR ≤ -20 dB the resolution percentage is almost zero.

In Fig. 5a, the RMSE of DOA estimation using SPICE and MLE is plotted against the number of snapshots N for a fixed SNR $= -2$ dB. The MLE achieves the CRB for $N \geq 20$ samples, whereas the SPICE method is above the CRB because of the bias resulting from the nature of the SSR approaches [36]. In Fig. 5b, the source resolution percentage is plotted against N. Observe that the SPICE and the MLE achieve 100% resolution percentage for $N \geq 20$.

In Fig. 6a and Fig. 6b, for a fixed SNR of -2 dB and fixed number of samples $N = 50$, the number of sources L is changed. The source DOAs are chosen in order from the set $\{15°, -15°, 30°, -30°, 45°, -45°, 60°, -60°\}$. Observe in Fig. 6a that for small number of sources $L \leq 4$ the MLE and the SPICE achieves the CRB. In Fig. 6b, it can be seen that for $L \leq 5$ both the SPICE and the MLE methods are always able to identify the sources. We remark that since $M_k = 2$ for $k = 1, \ldots, K$ none of the subarrays can individually identify more than one source, however, with our proposed methods, which exploit the diverse structure of the subarrays, up to $L = 5$ sources can be identified.

In the following, we investigate the performance of the MLE and SPICE considering $L = 2$ correlated sources. In Fig. 7a, the number of samples is fixed to $N = 50$ and the RMSE for DOA estimation of the MLE is plotted against SNR for different values of the correlation factor $\epsilon = 0, 0.3, 0.6$, and $\epsilon = 1$. Note that the RMSE decreases by increasing ϵ. For coherent sources, i.e., $\epsilon = 1$, the RMSE approaches zero for high SNR, which is in correspondence to our discussion in Section 4.2. The averaged performance of the SPICE for the same scenario is shown in Fig. 7b. Note that the SPICE method is robust against the assumption of correlated sources, i.e., the performance of SPICE does not degrade much with the increased correlation between the sources, see [43].

6. Summary and Conclusions

In this paper, we considered non-coherent DOA estimation using partly calibrated arrays. The presentation is focused on the case where none of the subarrays is able to individually identify all the sources. A sufficient condition for uncorrelated sources identifiability using non-coherent processing is presented. We proved that using non-coherent processing it is possible to identify more sources than each subarray individually can. Moreover, the CRB for non-coherent processing is derived and its behaviour at high SNR is analyzed. Two methods, namely the MLE and SPICE, are proposed to estimate the DOAs from the sample covariance matrices received from all subarrays. Using the simulations, the performance of the MLE is shown to achieve the derived CRB.

7. Acknowledgements

The project ADEL acknowledges the financial support of the Seventh Framework Programme for Research of the European Commission under grant number: 619647.

A. Proof of Theorem 1

The proof of Theorem 1 consists in showing the sufficiency of the condition (23). We remark that for fully calibrated arrays using coherent processing a bound on the maximum number of identifiable sources is introduced in [22]. This bound is not applicable in our case since in [22] the covariance matrix of the whole array is assumed to be available and thus the bound is introduced using the rank of the matrix $\boldsymbol{V}$ and not $\breve{\boldsymbol{V}}$ as is this paper. Our proof of the bound is similar in spirit to that of [22].

A.1. Sufficiency of (23)

In this section, we prove that if $\breve{\boldsymbol{V}}(\boldsymbol{\theta})\boldsymbol{\lambda} = \breve{\boldsymbol{V}}(\boldsymbol{\theta}')\boldsymbol{\lambda}'$ and $L \leq \lfloor \frac{\rho}{2} \rfloor$ then $\boldsymbol{\theta} = \boldsymbol{\theta}'$.

Proof. Assume that there are $q \leq L \leq \lfloor \frac{\rho}{2} \rfloor$ entries which occur in both DOA vectors $\boldsymbol{\theta}$ and $\boldsymbol{\theta}'$. Then, $\boldsymbol{\theta}$ and $\boldsymbol{\theta}'$ can be split as $\boldsymbol{\theta} = [\boldsymbol{\theta}_1^T, \boldsymbol{\theta}_2^T]^T$ and $\boldsymbol{\theta}' = [\boldsymbol{\theta}_1'^T, \boldsymbol{\theta}_2'^T]^T$ such that $\boldsymbol{\theta}_1 = \boldsymbol{\theta}_1' \in \mathbb{R}^{q \times 1}$ and that the DOAs $\boldsymbol{\theta}_2$ and $\boldsymbol{\theta}_2'$ are all different. Moreover, we define $\boldsymbol{\lambda} = [\boldsymbol{\lambda}_1^T, \boldsymbol{\lambda}_2^T]^T$ and $\boldsymbol{\lambda}' = [\boldsymbol{\lambda}_1'^T, \boldsymbol{\lambda}_2'^T]^T$, where $\boldsymbol{\lambda}_1, \boldsymbol{\lambda}_2, \boldsymbol{\lambda}_1'$, and $\boldsymbol{\lambda}_2'$ contain the power of the sources corresponding to the DOAs $\boldsymbol{\theta}_1, \boldsymbol{\theta}_2, \boldsymbol{\theta}_1'$ and $\boldsymbol{\theta}_2'$, respectively. Thus, the assumption that $\breve{\boldsymbol{V}}(\boldsymbol{\theta})\boldsymbol{\lambda} = \breve{\boldsymbol{V}}(\boldsymbol{\theta}')\boldsymbol{\lambda}'$ can be written as

$$[\breve{\boldsymbol{V}}(\boldsymbol{\theta}_1), \breve{\boldsymbol{V}}(\boldsymbol{\theta}_2)][\boldsymbol{\lambda}_1^T, \boldsymbol{\lambda}_2^T]^T = [\breve{\boldsymbol{V}}(\boldsymbol{\theta}_1'), \breve{\boldsymbol{V}}(\boldsymbol{\theta}_2')][\boldsymbol{\lambda}_1'^T, \boldsymbol{\lambda}_2'^T]^T. \tag{46}$$

Since $\breve{\boldsymbol{V}}(\boldsymbol{\theta}_1) = \breve{\boldsymbol{V}}(\boldsymbol{\theta}_1')$, (46) can be rearranged as

$$[\breve{\boldsymbol{V}}(\boldsymbol{\theta}_1), \breve{\boldsymbol{V}}(\boldsymbol{\theta}_2), \breve{\boldsymbol{V}}(\boldsymbol{\theta}_2')][\boldsymbol{\lambda}_1^T - \boldsymbol{\lambda}_1'^T, \boldsymbol{\lambda}_2^T, -\boldsymbol{\lambda}_2'^T]^T = 0. \tag{47}$$

Next, we distinguish between the following two cases:

1. $q = L$: In this case $\boldsymbol{\theta}_1 = \boldsymbol{\theta} = \boldsymbol{\theta}'$ and $\boldsymbol{\lambda} = \boldsymbol{\lambda}'$ is a unique solution to (47), i.e., in this case the DOAs are uniquely identifiable.

2. $q < L$: In this case, the matrix $[\breve{\boldsymbol{V}}(\boldsymbol{\theta}_1), \breve{\boldsymbol{V}}(\boldsymbol{\theta}_2), \breve{\boldsymbol{V}}(\boldsymbol{\theta}_2')]$ contains $2L - q$ columns corresponding to different DOAs. Since $q < L$ and $L \leq \lfloor \frac{\rho}{2} \rfloor$ the inequality $2L - q \leq 2L \leq \rho$ holds. Consequently, the matrix $[\breve{\boldsymbol{V}}(\boldsymbol{\theta}_1), \breve{\boldsymbol{V}}(\boldsymbol{\theta}_2), \breve{\boldsymbol{V}}(\boldsymbol{\theta}_2')]$ is full rank and (47) can only be satisfied, in this case, if $[\boldsymbol{\lambda}_1^T - \boldsymbol{\lambda}_1'^T, \boldsymbol{\lambda}_2^T, -\boldsymbol{\lambda}_2'^T]^T = 0$. However, this is not possible since it implies that $\boldsymbol{\lambda}_2' = \boldsymbol{\lambda}_2 = 0$, i.e., the sources corresponding to the DOAs $\boldsymbol{\theta}_2$ and $\boldsymbol{\theta}_2'$ have zero power.

Thus, (47) can only be satisfied in case 1) which proves the theorem.

□

References

[1] H. L. Van Trees. Detection, Estimation, and Modulation Theory - Part IV: Optimum Array Processing. Wiley-Interscience, 2002

[2] R. Schmidt. Multiple emitter location and signal parameter estimation. *IEEE Transactions on Antennas and Propagation*, 34(3):276–280, Mar. 1986.

[3] A. Barabell. Improving the resolution performance of eigenstructure-based direction-finding algorithms. *IEEE International Conference on Acoustics, Speech and Signal Processing (ICASSP)*, vol. 8. IEEE, 1983, pp. 336339.

[4] P. Stoica and K. C. Sharman. Maximum likelihood methods for direction-of-arrival estimation. *IEEE Transactions on Acoustics, Speech and Signal Processing*, 38(7):1132–1143, July 1990.

[5] M. Viberg and B. Ottersten and T. Kailath. Detection and estimation in sensor arrays using weighted subspace fitting. *IEEE Transactions on Signal Processing*, vol. 39, no. 11, pp. 24362449, Nov. 1991.

[6] R. Roy and T. Kailath. ESPRIT-estimation of signal parameters via rotational invariance techniques. *IEEE Transactions on Acoustics, Speech and Signal Processing*, 37(7):984–995, Nov. 1989.

[7] M. Pesavento, A. B. Gershman, and K. M. Wong. Direction finding in partly calibrated sensor arrays composed of multiple subarrays. *IEEE Transactions on Signal Processing*, 50(9):2103–2115, Sept. 2002.

[8] P. Parvazi and M. Pesavento and A. B. Gershman. Direction-of-arrival estimation and array calibration for partly-calibrated arrays. In *IEEE International Conference on Acoustics, Speech and Signal Processing (ICASSP)*, Prague, Czech Republic, May 2011, pp. 25522555.

[9] P. Parvazi and M. Pesavento. A new direction-of-arrival estimation and calibration method for arrays composed of multiple identical subarrays. In *IEEE International Workshop on Signal Processing Advances in Wireless Communications (SPAWC)*, pages 171–175, San Francisco, CA, USA, June 2011.

[10] P. Stoica and A. Nehorai and T. Söderström. Decentralized array processing using the MODE algorithm. *Circuits, Systems and Signal Processing*, vol. 14, no. 1, pp. 1738, 1995.

[11] M. Wax and T. Kailath. Decentralized processing in sensor arrays. *IEEE Transactions on Acoustics, Speech and Signal Processing*, 33(5):1123–1129, Oct. 1985.

[12] D. Rieken and D. Fuhrmann. Generalizing MUSIC and MVDR for multiple noncoherent arrays. *IEEE Transactions on Signal Processing*, vol. 52, no. 9, pp. 23962406, Sept 2004.

[13] T. Söderström and P. Stoica. Statistical analysis of decentralized MUSIC. *Springer Circuits, Systems and Signal Processing*, vol. 11, no. 4, pp. 443454, Dec. 1992.

[14] D. D. Lee and R. L. Kashyap and R. N. Madan. Robust decentralized direction-of-arrival estimation in contaminated noise. *IEEE Transactions on Acoustics, Speech and Signal Processing*,vol. 38, no. 3, pp. 496505, Mar. 1990.

[15] W. Suleiman and P. Parvazi. Search-free decentralized direction-of-arrival estimation using common roots for non-coherent partly calibrated arrays. In *IEEE International Conference on Acoustics, Speech and Signal Processing (ICASSP)*, pages 2292–2296, May 2014.

[16] J. Sheinvald and M. Wax. Direction finding with fewer receivers via time-varying preprocessing. In *IEEE transactions on signal processing*, vol. 47, no. 1, pp. 29, 1999.

[17] H. Kim and A. M. Haimovich and Y. C. Eldar. Non-coherent direction of arrival estimation from magnitude-only measurements. In *IEEE Signal Processing Letters*, vol. 22, no. 7, pp. 925929, 2015.

[18] A. Scaglione, R. Pagliari, and H. Krim. The decentralized estimation of the sample covariance. In *Asilomar Conference on Signals, Systems, and Computers*, pages 1722–1726, Pacific Grove, CA, USA, Oct. 2008.

[19] W. Suleiman and M. Pesavento and A. M. Zoubir. Performance analysis of the decentralized eigendecomposition and ESPRIT algorithm. In *IEEE Transactions on Signal Processing*, vol. 64, no. 9, pp. 23752386, May 2016.

[20] A. Graham. Kronecker products and matrix calculus: with applications. ser. Ellis Horwood series in mathematics and its applications. Horwood, 1981.

[21] Y. I. Abramovich and N. K. Spencer and A. Y. Gorokhov. Resolving manifold ambiguities in direction-of-arrival estimation for nonuniform linear antenna arrays. In *IEEE Transactions on Signal Processing*, vol. 47, no. 10, pp. 26292643, Oct 1999.

[22] B. Hochwald and A. Nehorai. Identifiability in array processing models with vector-sensor applications. In *IEEE Transactions on Signal Processing*, vol. 44, no. 1, pp. 8395, 1996.

[23] A. Stegeman and N. D. Sidiropoulos. On Kruskal's uniqueness condition for the Candecomp/Parafac decomposition. In *Linear Algebra and its applications*, vol. 420, no. 2, pp. 540552, 2007.

[24] J. B. Kruskal. Three-way arrays: rank and uniqueness of trilinear decompositions, with application to arithmetic complexity and statistics. In *Linear Algebra and its applications*, vol. 18, no. 2, pp. 95138, 1977.

[25] M. Wax and I. Ziskind. On unique localization of multiple sources by passive sensor arrays. In *IEEE Transactions on Acoustics, Speech and Signal Processing*, vol. 37, no. 7, pp. 9961000, 1989.

[26] P. J. Schreier and L. L. Scharf. Statistical signal processing of complex-valued data: the theory of improper and noncircular signals. Cambridge University Press, 2010.

[27] S. P. Boyd and L. Vandenberghe. Convex optimization. Cambridge university press, 2004.

[28] J. Sheinvald and M. Wax and A. J. Weiss. On the achievable localization accuracy of multiple sources at high SNR. IEEE Transactions on Signal Processing, vol. 45, no. 7, pp. 17951799, Jul 1997.

[29] K. M. Abadir and J. R. Magnus. Matrix algebra. Cambridge University Press, 2005, vol. 1.

[30] Y. I. Abramovich and D. A. Gray and A. Y. Gorokhov and N. K Spencer. Positive-definite Toeplitz completion in DOA estimation for nonuniform linear antenna arrays. I. fully augmentable arrays. IEEE Transactions on Signal Processing, vol. 46, no. 9, pp. 24582471, 1998.

[31] R. Tibshirani. Regression shrinkage and selection via the LASSO. Journal of the Royal Statistical Society. Series B (Methodological), pp. 267288, 1996.

[32] D. L. Donoho, M Elad, and V. N. Temlyakov. Stable recovery of sparse overcomplete representations in the presence of noise. IEEE Transactions on Information Theory, vol. 52, no. 1, pp. 618, 2006.

[33] D. L. Donoho and X. Huo. Uncertainty principles and ideal atomic decomposition. IEEE Transactions on Information Theory, vol. 47, no. 7, pp. 28452862, 2001.

[34] D. L. Donoho and Y. Tsaig. Fast solution of-norm minimization problems when the solution may be sparse. IEEE Transactions on Information Theory, vol. 54, no. 11, pp. 47894812, 2008.

[35] E. J. Candes and M. B. Wakin. An introduction to compressive sampling, . IEEE Signal Processing Magazine, vol. 25, no. 2, pp. 2130, 2008.

[36] D. Malioutov and M. Çetin and A. S. Willsky. A sparse signal reconstruction perspective for source localization with sensor arrays. IEEE Transactions on Signal Processing, vol. 53, no. 8, pp. 30103022, 2005.

[37] M. M. Hyder and K. Mahata. Direction-of-arrival estimation using a mixed norm approximation. IEEE Transactions on Signal Processing, vol. 58, no. 9, pp. 46464655, 2010.

[38] C. Steffens and P. Parvazi and M. Pesavento. Direction finding and array calibration based on sparse reconstruction in partly calibrated arrays. in IEEE Sensor Array and Multichannel Signal Processing Workshop (SAM), 2014, pp. 2124.

[39] J. Yin and T. Chen. Direction-of-arrival estimation using a sparse representation of array covariance vectors. IEEE Transactions on Signal Processing, vol. 59, no. 9, pp. 44894493, 2011.

[40] M. Atashbar and M. H. Kahaei. Direction-of-arrival estimation using AMLSS method. IEEE Latin America Transactions, vol. 10, no. 5, pp. 20532058, 2012.

[41] I. CVX Research. CVX: Matlab software for disciplined convex programming, version 2.0. , http://cvxr.com/cvx, Aug. 2012.

[42] C. Steffens and M. Pesavento and M. E. Pfetsch. A compact formulation for the $\ell_{2,1}$ mixed-norm minimization problem. arXiv:1606.07231, 2016.

[43] P. Stoica and P. Babu and J. Li. SPICE: a sparse covariance-based estimation method for array processing. IEEE Transactions on Signal Processing, vol. 59, no. 2, pp. 629638, 2011.